ACS EARTH AND SPACE CHEMISTRY

Article

http://pubs.acs.org/journal/aesccq

Microbes Facilitate Mineral Deposition in Bioelectrochemical Systems

A. Gartman,*[,†,§] A. Picard,[†] H. C. Olins,[†] N. Sarode,[†] D. R. Clarke,[‡] and P. R. Girguis*[,†]

[†]Department of Organismic and Evolutionary Biology, Harvard University, 16 Divinity Avenue, Cambridge, Massachusetts 02138, United States

[‡]John A. Paulson School of Engineering and Applied Sciences, Harvard University, 29 Oxford Street, Cambridge, Massachusetts 02138, United States

Supporting Information

ABSTRACT: Hydrothermal chimneys are striking, characteristic features of marine hydrothermal vents. These chimneys are dynamic environments occupied by a diversity of microbes whose distribution is typically concordant with mineralogy and temperature. Recent studies indicate that these chimney assemblages are conductive and present the possibility that microbial extracellular electron transfer may occur through these minerals, linking spatially separated electron donors and acceptors. Here we explore the relationships among biology, mineralogy, and electric potential in hydrothermal systems using crushed hydrothermal chimney as inoculum in high (75 °C) and low (30 °C) temperature bioelectrical systems. All experiments with live microbial communities incubated in the presence of a poised electrode resulted in enhanced mineral deposition relative to (A) a live, open circuit (not poised) electrode, or (B) dead microbial communities in the presence of a poised electrode. Microbial abundance increased in both high- and low-temperature treatments, dominated by taxa allied to the Deferribacterales on the high-temperature treatment electrode, and Chromatiales and Campylobacterales on the low-temperature treatment electrodes. Here we discuss the results of these experiments and consider the implications of these observations for the role that microorganisms may play in the formation of metal-rich hydrothermal chimneys.

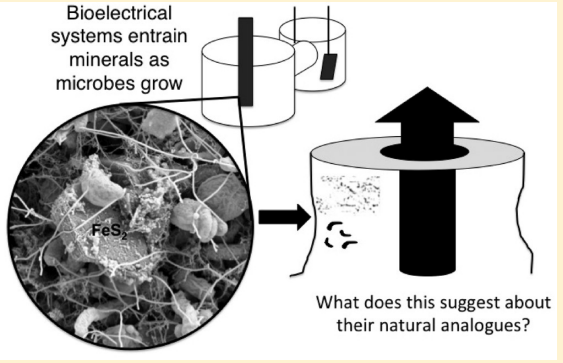

KEYWORDS: *Microbe-mineral interactions, hydrothermal chimney, exoelectrogen, biofilm, metal sulfide*

INTRODUCTION

Hydrothermal vent chimneys are conspicuous structures that are common around deep-sea hydrothermal vents. These features are combinations of minerals including pyrite, chalcopyrite, sphalerite (metal sulfides), barite, and anhydrite (barium and calcium sulfate[1]), assembled in various grain sizes, pore spaces, and connectivities.[2] Vent chimney "walls" exhibit strong redox gradients, as hot, reduced metal-rich fluid in the interior mixes with cold, oxygenated seawater, with the two fluids separated by actively forming porous mineral precipitates. Many metal sulfides are known semiconductors, and resistivities of seawater-immersed hydrothermal chimneys from diverse systems vary from 10^{-7} to 7 Ωm and trend with mineralogy, porosity, and likely mineral texture; broadly, Cu- and Fe-rich sulfides exhibit the lowest resistivities (highest conductivities).[3] Metal-like resistivities measured from the interior to the exterior of a chimney collected from Mariner, Lau Basin, are suggested to occur as a result of nanoparticulate inclusions or mineral doping to the host mineral.[4]

The microbial communities inhabiting these chimneys are diverse and have been observed to zone with mineralogy.[5,6] In active, high temperature chimneys, cells are most abundant toward the exterior (where temperatures are habitable) and can reach densities of $>10^8$ cells/g.[5] Broadly speaking, bacteria are more abundant in the cooler, exterior sections, whereas archaea are more prevalent in the warmer habitable zones. Zonation also occurs even when the systems are inactive.[6] A biogeochemical reaction-transport model of a chimney indicates that microbial activity is likely to be highest in the hottest-habitable central regions and suggests that peak metabolic rates occur where the temperature is greater than 50 °C, often between one and two centimeters from the inner chimney wall.[7] For example, in chimneys in Middle Valley, Juan de Fuca, the highest rates of microbial sulfate reduction have been measured at 90 °C, and different rates of sulfate reduction between sites were not easily explained by geochemistry or biomass.[8] However, the relationships between temperature and microbial activity are complex and other factors (e.g., oxidant availability and organic carbon load in the bottom water as well as competition for space and resources) can influence the distribution of microbes and their rates of activity.[8,9]

Received: April 18, 2017
Revised: June 5, 2017
Accepted: June 9, 2017
Published: June 9, 2017

DOI: 10.1021/acsearthspacechem.7b00042
ACS Earth Space Chem. 2017, 1, 277−287

In recent years, an increasing number of bacteria in a variety of environments have been characterized as capable of transferring electrons extracellularly through several mechanisms[10,11] including soluble redox shuttles, direct contact with the electrode, and microbial "nanowires". Extracellular electron transfer (EET) enables microbes to access electron donors or acceptors that they may be spatially separated from, or that may be insoluble. *Shewanella oneidensis*, *Geobacter sulfurreducens*, and *Therminocola potens* are three of the best-studied exoelectrogens[11] and are genetically and metabolically quite different, demonstrating that extracellular electron transfer occurs across phyla (γ- and δ- Proteobacteria; Firmicutes) and through diverse mechanisms. Bioelectrical systems have been used to study these taxa, through presenting an electrode as either an electron donor or acceptor, and mimicking the minerals that may be encountered in situ.

Although the external electron transferring capability of exoelectrogens has been suggested to be linked to mineral oxidation and reduction, and electrodes have been used to enrich for lithotrophs from marine environments,[12] the processes of lithotrophy and EET with an electrode are different enough from one another that natural "geobatteries[13]" have been proposed as a more direct analog to a laboratory electrode, as they present a more sustained source of current.[11] In nature, sustained current flow has been measured in cold seep sediments,[14,15] as well as hydrothermal vents.[16] While some studies have considered the role of minerals in the zonation of hydrothermal vent microbes, the converse, the role of microbes in the mineral deposition and potential zonation of hydrothermal chimneys, has not been as thoroughly examined. For example, the role of electrical conductivity in the microbe−mineral zonation of hydrothermal chimneys has not been explored and whether biofilms enhance conductivity of chimneys is also unknown. To better understand the interplay between chimney mineralogy, electrical interactions, and vent microbial activity, we conducted a series of experiments in which we examined the nature and rate of mineral growth and deposition on poised and open-circuit electrodes (no imposed potential) in the presence of live and dead vent microbial communities. The poised electrodes are aimed at mimicking the electrical potentials observed during in situ measurements. Post-treatment, we conducted geochemical, mineralogical, and microbial phylogenetic analyses to examine differences among the treatments. Here we discuss these findings and their implications for the role of microbes in hydrothermal vent chimney deposition.

EXPERIMENTAL SECTION

Equipment and Supplies Used for Bioelectrochemical Systems. Our experiments were designed to assess microbe−mineral−electrochemical reactions relevant to hydrothermal vents. To assess the diversity of regimes occurring in these systems, we chose to test two temperatures (30 and 75 °C) and two potentials that could occur in the hydrothermal vent zone (195−218 mV vs Ag/AgCl (403−428 mV vs standard hydrogen electrode (SHE)), with a natural mineral/microbial assemblage. We set up three-electrode systems across a two-chambered borosilicate glass reactor using a graphite rod as the working electrode, a saturated Ag/AgCl reference electrode, and a graphite cloth and titanium wire counter electrode (SI Figure 1). The reactor was divided by a Nafion membrane purchased from the Fuel Cell Store (part no. 591239). The working electrode was a high-temperature conductive graphite rectangular cuboid (6 mm/side × 50 mm length immersed in fluid (surface area 1.24 × 10^{-3} m^2); McMaster Carr Inc. 1763T31) and was epoxied (WestMarine Inc.) into a butyl rubber stopper, which was used to seal the anoxic, working chamber of the reactor. An Ag/AgCl reference electrode filled with saturated KCl, a graphite cloth (AvCarb Materials), and titanium wire counter electrode constructed with 1 mm diameter titanium wire were threaded through a second rubber stopper and placed in the oxic counter chamber. Gamry Interface 1000 potentiostats were used to poise the electrodes at a fixed potential and log current as a function of time.

Sample Collection and Preparation. The inoculum used for both experiments was collected from Bio9, EPR 9°N (9°50′18.75″ N, 104°17′29.03″W) in Nov 2014 by HOV *Alvin*, dive D4768, during cruise AT 26-23 on board the RV *Atlantis*. Samples were collected by breaking off a piece of high temperature chimney from an active black smoker using the Alvin manipulator. Upon recovery to the surface vessel, we noted that the chimney exhibited a typical gradient from copper−iron rich sulfides in the inner wall, through zinc and iron rich sulfides, and an anhydrite dominated outer wall (SI Figure 2). Recovered chimney samples were placed in anoxic seawater with ∼5 mM $\sum H_2S$ at pH ∼ 7 and stored in glass gastight jars (Mason Inc.) at 4 °C until experiments were begun. For the 30 °C experiment, approximately two months elapsed between the time of sample collection and the time of experiment; for the 75 °C experiment, approximately five months elapsed between collection and the start of the experiment.

Prior to the experiment, pieces of hydrothermal chimney were removed from the sulfidic seawater jar and crushed with a sterile mortar and pestle in an anaerobic chamber (Coy Laboratories Inc.). For the "live" treatments, a ∼ 3 mL scoop of hydrothermal chimney was introduced to the working cell in an anaerobic chamber. For the "control" treatments, which are intended to assess the abiotic processes in the system, the crushed chimney scoop was autoclaved for >30 min prior to being added to the reactors. After addition of the mineral slurry, the working chamber was closed, and within an hour of assembly was hooked up to its relevant potentiostat.

Experimental Design. Individual bioelectrochemical systems (or BESs) were operated at both 30 and 75 °C. The 30 °C temperature experiments were maintained in a 30 °C room, whereas the 75 °C experiment was immersed in a 5 L metal bead bath (Lab Armor). Two potentials, 195 and 218 mV, were tested at 30 °C (all potentials discussed here are vs. Ag/AgCl). These potentials were chosen to be similar to the midpoint potential of pyrite at pH values relevant at hydrothermal vents (between 5 and 6[17]) and were chosen to be slightly different in order to acknowledge that potential values occurring in natural systems are not static. The temperatures represent two possible thermal regimes that are common at hydrothermal vents. After observing similar mineralogical results for both potentials at 30 °C (Results), we chose to solely test the 195 mV in the 75 °C experiments. At each potential, one BES was inoculated with chimney subsamples that were replete with living hydrothermal vent microbes, while the other BES was inoculated with chimney subsamples that had been killed by autoclaving. Each working cell was filled with anaerobic medium DSMZ 195C,[18] which contained 21 mM Na_2SO_4, 1.5 mM KH_2PO_4, 5.6 mM NH_4Cl, 360 mM NaCl, 15.3 mM $MgCl_2$, 6.7 mM KCl, 1 mM $CaCl_2$, 47 mM $NaHCO_3$, and 28 mM lactate. The volume of fluid in the reactors for all experiments was 160 mL.

DOI: 10.1021/acsearthspacechem.7b00042
ACS Earth Space Chem. 2017, 1, 277−287

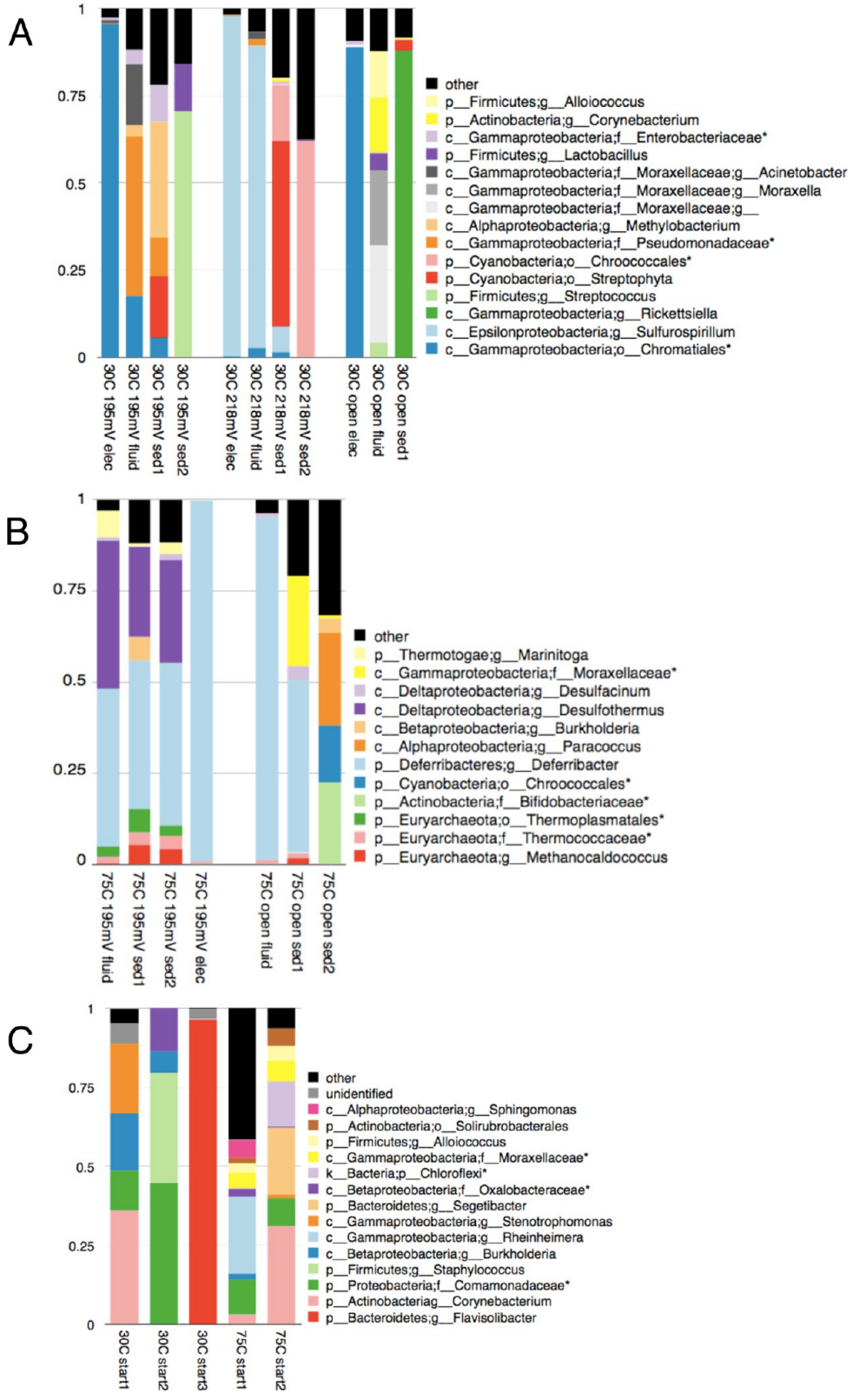

Figure 1. Microbial community composition from16S rRNA gene analysis. (A) Results of the 30 °C live experiments, at 34 days. (B) The 16S results of the 75 °C live experiments at 13 days. (C) The 16S results of the crushed sediments used as inoculum at the start of the both experiments. In panels B and C, "open" refers to experiments performed with no imposed potential.

Trace Mineral Supplement MD-TMS and Vitamin Stocks MD-VS, (both by ATCC Inc.) were added at concentrations of 1 mL per liter of medium. At the start of the experiment, the solution was brought to a concentration of 1.5 mM Fe, 40 μM Cu, 100 μM Zn, and 120 μM Mn, and 5 mM Na_2S to approximate the high metal and sulfide concentrations at hydrothermal vents. Additional sulfide was added every 3−8 days in all treatments to maintain the sulfide concentration at

DOI: 10.1021/acsearthspacechem.7b00042
ACS Earth Space Chem. 2017, 1, 277−287

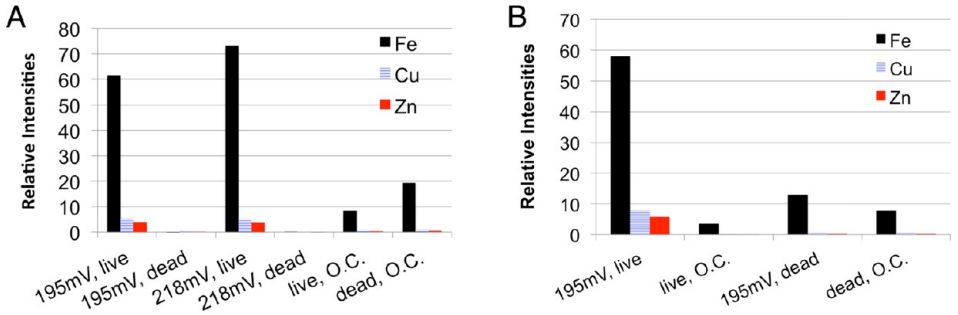

Figure 2. XRF results from the experiments at 30 °C (A) and 75 °C (B) and showing that the live, poised electrodes in each experimental set exhibited more deposition than either live, open circuit, or dead poised. O.C. refers to experiments conduced with no imposed potential.

~5 mM, ensuring that the working chamber remained anoxic. The counter chamber was filled with filter-sterilized seawater and saturated with air via bubbling, resulting in oxygen concentrations of ~195 and ~110 μM in the 30° and 75 °C treatments, respectively. The pH of the medium prior to the addition of sulfide was 6.9–7.1. At the end of the experiments, pH values were ~7.9–8. The treatments at 30 °C ran for 34 days and 75 °C experiments ran for 13 days and were stirred continually over the course of the experiment.

X-ray Diffraction (XRD). Mineralogy of the chimney sulfide slurries, prior to and upon completion of the treatments, was measured via XRD at the Harvard Department of Chemistry and Chemical Biology X-ray Laboratory. Powdered chimney subsamples were dried under nitrogen then subjected to XRD using a Bruker D2 Phaser with Cu kα radiation. Scans were collected from 5 to 70° 2θ with an increment of 0.01 and 5 s per step. Mineralogical deposits on the electrode were assessed at the end of the experiment using a Bruker D8 Discover using a 2D detector in XRD 2 mode. XRD 2 scans were collected from 10 to 100° 2θ. EVA D3 software was used to search for phases and perform semiquantitative analysis. The XRD analysis prior to the start of the experiment was performed on a sample that had not been autoclaved.

Scanning Electron Microscopy and Energy Dispersive X-ray Spectroscopy (SEM/EDS). SEM was performed using a Zeiss SupraVP55 FE-SEM at the Harvard Center for Nanoscale Systems. High-resolution imaging was performed at 5 kV using an Everhart-Thornley detector. Elemental analysis performed at 20 kV using an EDAX detector. For analysis of mineral morphology, samples were dried in a glovebox under nitrogen. For analysis of microbial growth, samples were fixed with glutaraldehyde (final concentration of 2.5%), ethanol dehydrated, and critical point dried (CPD). All samples were coated with 5 nm Pd/Pt prior to microscopy. EDAX Genesis was used for elemental analysis.

Confocal Laser Scanning Microscopy (CLSM). Fluorescent probes (Invitrogen Inc.) were used to label nucleic acids (Sybr Green), peptidoglycan (wheat germ agglutinin Alexa Fluor 555), and lipids (FM4-64) on the electrode. The electrode piece was stained with the fluorescent probes for ~30 min and rinsed with phosphate-buffered saline (1× PBS). It was then immersed in 1× PBS in a Nunc Lab-Tek II chambered coverglass and imaged using an inverted confocal laser scanning microscope (LSM 880, Zeiss) at the Harvard Center for Biological Imaging. Z-stacks of images were acquired with a 100× oil immersion lens. The fluorescence signal was excited using lasers (488 nm for nucleic acids and 561 nm for peptidoglycan and lipids) and recorded sequentially in separate channels. The reflection signal of the mineral surface (at 405 nm) was also recorded. Alexa Fluor 555 specifically targets the residues of *N*-acetylglucosamine and *N*-acetyl muramic acid. Only the poised electrode from the 75 °C trial was investigated using CLSM.

X-ray Fluorescence (XRF). XRF of the electrodes was performed at the Harvard Center for Nanoscale Systems using a SPECTRO XEPOS XRF. Molybdenum was used as the secondary target. Synthesized and natural pyrite, natural chalcopyrite, natural sphalerite, and natural anhydrite were used to calibrate elemental ratios and XRF results are presented in terms of relative intensities based on normalizing the absolute intensities to these calibrations.

16S rRNA Extraction, Sequencing, and Analysis. DNA extractions were performed using MoBio PowerSoil DNA isolation kit. The sample used to represent the inoculum (T = 0) was crushed chimney material frozen at −80 °C at the time of inoculation for each experiment (called "start" in Figure 1, SI Figure 3). The postincubation material consisted of scrapings from the electrode (represented as "elec" in Figure 1, SI Figure 3), the fluid in the chamber at the end of the experiment ("fluid" in Figure 1, SI Figure 3), and the mineral precipitate remaining at the bottom of the chamber at the end of the experiment ("sed" in Figure 1, SI Figure 3), collected at the end of each experiment, 34 days for the 30 °C trials and 13 days for the 75 °C trials. All were frozen at −80 °C immediately after sampling until the time of extraction.

The extraction procedure is briefly described as follows: Either crushed hydrothermal sulfide chimney, up to 1 mL of fluid from the reactor, or scrapings from one face of the working electrode was added to a PowerSoil bead-beating tube. DNA was then extracted using a modified MoBio PowerSoil extraction protocol.[19] Where material was sufficient, duplicate or triplicate extractions were performed and sequenced separately (these are indicated in Figure 1 and SI Figure 3 by sequential numbers). After extraction, DNA was sent to Research and Testing Laboratories (RTLGenomics) for 16S rRNA gene amplification using Earth Microbiome Project (EMP) primers (universal bacteria/archaeal primers 515F/806R). The amplified gene regions were then sequenced on Illumina MiSeq to generate paired end 250bp reads.[20] RTLGenomics also completed taxonomic identification, including chimera checking using their standard protocol. Briefly, merged sequences were clustered into OTUs using the UPARSE algorithm[21] and OTUs were identified with the USEARCH algorithm using NCBI database as reference. Chimera checking was performed using a de novo method in UCHIME.

For further confidence in taxonomic identification, post- QC sequences generated by RTL's standard protocol were

DOI: 10.1021/acsearthspacechem.7b00042
ACS Earth Space Chem. 2017, 1, 277–287

processed through QIIME pipeline v1.9.0.[22] The merged reads were first screened for additional chimeras using Usearch6.1,[23] which performs both de novo and reference-based detection. An additional 19 500 chimeras were detected and removed from further analysis. The nonchimeric sequences were then clustered into OTUs at 97% sequence similarity with open reference OTU picking method implementing Ucluster algorithim[23] and PyNast for alignment.[22] The reference database used was the August 2013 release of Greengenes.[24] For all samples, the taxonomy assigned by QIIME is discussed unless otherwise indicated. Nonmetric multidimensional scaling was performed using Mothur[25] and was used to visualize beta diversity patterns in microbial community structure over spatial and temporal scales for the experiments (SI Figure 4).

RESULTS

Summary. In all experiments, treatments in which the inoculum was live and the electrode was poised resulted in the greatest metal sulfide deposition on the electrode, which was determined quantitatively through XRF with respect to iron, copper, and zinc (Figure 2) with minerals identified through XRD (Table 1). For all three experiments, phylogenetic community analyses revealed strong enrichment on the working electrode; >97% Campylobacterales at 30 °C and 218 mV, >95% *Chromatiales sp.* at 30 °C and 195 mV, and >97% Deferribacterales at 75 °C (these percentages are the proportion of 16 rRNA gene fragments attributable to these taxa). SEM results confirm the mineral deposition in the live experiments and the presence of a biofilm in the 75 °C experiment (Figures 3 and 4, respectively). The results obtained from CLSM further demonstrate the spatial relationship of lipids, DNA, and polysaccharides in the biofilm in the 75 °C experiment (Figure 5). The high-temperature experiment resulted in the continuous and sustained production of current, which is not typical of solely abiotic interactions[14] but rather is consistent with an active community of exoelectrogenic microbes associated with the electrode and, potentially, the deposited minerals. For the experiments conducted at 30 °C, both poised, live electrodes (195 and 218 mV) had more metal sulfide deposition, observed via SEM and confirmed via XRF (Figures 2 and 3) than dead or open circuit controls, but current generation was inconclusive at both potentials (Figure 6). At both temperatures, the metal sulfide minerals deposited upon the electrodes appeared to consist of metal sulfide minerals that were added to the BES in the initial inoculum, as opposed to new sulfide mineral formation.

Table 1. Major Parameters and Results for All Experimental Trials, Including Temperature, Live or Dead, Potential, Length of Experiment, Minerals Deposited on the Electrode, and Whether Cells or a Biofilm Were Observed on the Electrode[a]

T (°C)	live or dead?	potential (mV)	no. of days	minerals on electrode[b]	cells visible (SEM)?	biofilm?
30	live	195	34	C, Py	y	n
30	dead	195	34	C# S#	n	n
30	live	218	34	C, Py, S, Sp	y	n
30	dead	218	34	C# S#	n	n
30	live	O.C.	34	C	n	n
30	dead	O.C	34	C S#	n	n
75	live	195	13	Sp, Cp, Ma, Py	y	y
75	dead	195	13	Cp, Ma, Py	n	n
75	live	O.C.	13	C#	y	n
75	dead	O.C.	13	C#	n	n

[a]O.C. refers to experiments that were conduced with no imposed potential. [b]C, calcite; MHC, monohydrocalcite; Py, pyrite; S, elemental sulfur; Sp, sphalerite; Cp, chalcopyrite; Ma, marcasite. [c]Minerals that are suggested based on EDS elemental ratios and consistency with XRD in sediment results but not confirmed via XRD on electrode. For "C#", this indicates the mineralogy could be any $CaCO_3$ species including MHC.

The 30 °C Experiment: Sediment and Solution Reactions. XRD results revealed that the starting material in these systems was primarily anhydrite (>80%) with gypsum as the next most abundant mineral (~11%), followed by chalcopyrite (SI Figure 5). At the end of the experiment, all of the gypsum had dissolved, along with some of the anhydrite. Sediments in the two dead, poised systems precipitated monohydrocalcite.

Beginning on day 24 of the experiment, a yellow color was visible in all of the working cells with the exception of the open circuit, dead system. On the basis of UV−vis spectrometry, which indicated an absorbance at 375 nm, this yellow color is tentatively ascribed to polysulfides. Although this was not demonstrated conclusively, the high concentration of sulfide added to the system, the oxidizing nature of the electrode, and the lack of organics to which the color could be attributed are all consistent with the presence of polysulfides.

The 30 °C Experiment: Electrode Deposition. For the experiments conducted at 30 °C, both poised, live electrodes (195 and 218 mV) had more metal sulfide deposition, observed via SEM and confirmed via XRF (Figures 2 and 3) than dead or open circuit controls. XRD revealed the dominant minerals on the two poised, live electrodes to be pyrite and calcite (Table 1). The two open circuit electrodes, both live and dead, contained only calcite, whereas the two dead, poised electrodes did not have minerals detectible via XRD, although SEM revealed elemental sulfur and a $CaCO_3$ phase (Table 1). The live, 195 mV experiment showed the most calcium deposition (SI Figure 6).

SEM performed after CPD demonstrated the presence of cells ~1 μm in length directly on the electrode surface for both live, poised trials (195 and 218 mV). Groups of cells were dispersed on the electrode, though no contiguous biofilm was observed (Figure 3a,b). No cells were found on the open circuit electrode, although there was microbial enrichment (detailed in following section). Current production at 195 mV was inconsistent and the live trial had slightly higher current than the kill control, whereas at 218 mV the kill control exhibited a slightly higher current than the live trial (Figure 6a,b).

Microbial Community Composition at 30 °C. The library representing the microbial community from the sediments, which served as the inoculum at the start of the experiments, was dominated by *Actinomycetales sp.*, *Burkholderiales sp.*, *Bacillales sp.*, and unclassified Bacteroidetes (three separate extractions; Figure 1c). At the end of the 30 °C live incubation with the electrode poised at 195 mV, the library representing the electrode community was instead heavily dominated (~95%) by *Chromatiales sp.*, while the fluid community in that reactor postincubation consisted mainly of *Chromatiales sp.* (18%) and *Pseudomonadales sp.* (63%). In contrast, the library representing the 30 °C electrode poised at 218 mV was heavily dominated (~97%) by Campylobacterales that RTL analysis suggests are allied to *Sulfurospirillum sp* (via

DOI: 10.1021/acsearthspacechem.7b00042
ACS Earth Space Chem. 2017, 1, 277−287

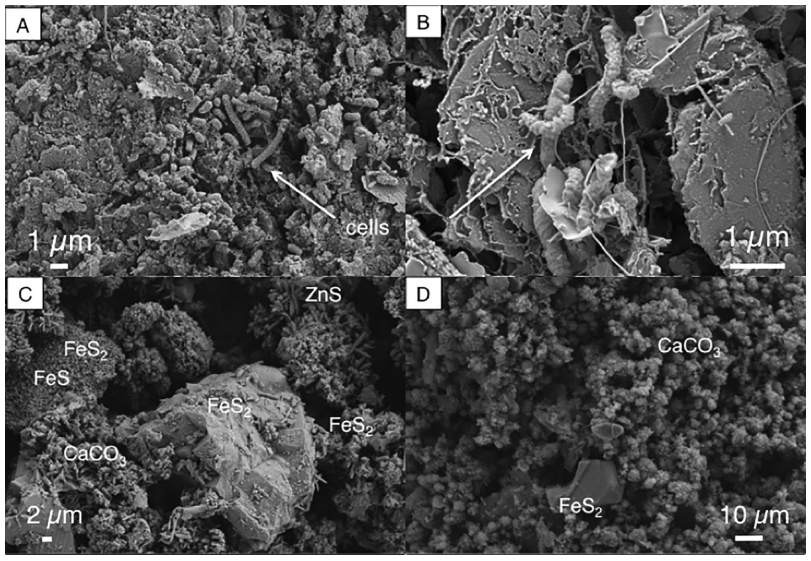

Figure 3. (A,B) Electron micrographs of the 30 °C live, poised electrode after critical point drying. (C,D) Same electrode dried under nitrogen and showing some metal sulfide deposition and abundant calcium carbonate deposition as measured via elemental ratios using EDS. In (A,B), the arrows denote the presence of cells.

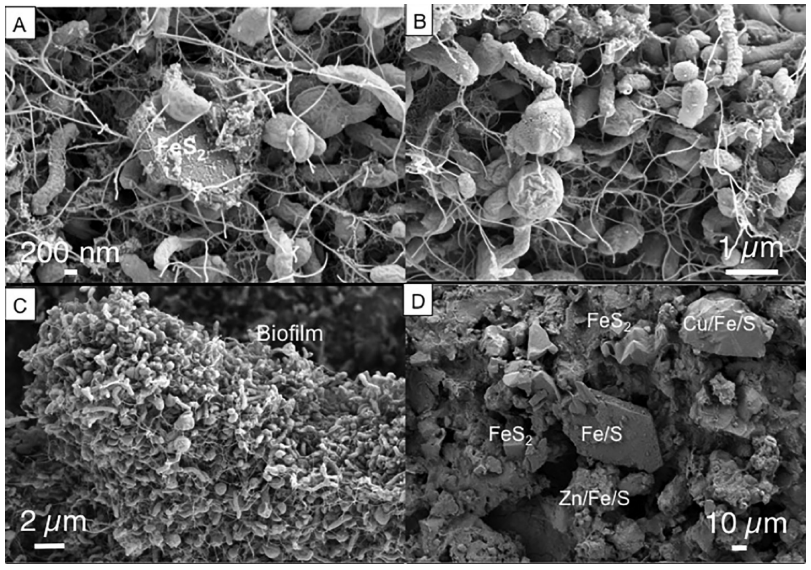

Figure 4. (A–C) electron micrographs of the 75 °C live, poised electrode after critical point drying. (D) The same electrode dried under nitrogen and showing abundant metal sulfide deposition.

the Krona pipeline;[26] Figure 1a). The postincubation fluids from this reactor were also dominated by Campylobacterales (87%). The library from the open circuit electrode community was also dominated (89%) by *Chromatiales sp.* postincubation, whereas those from open circuit sediment and fluid communities were predominantly *Legionellales sp.* (88%) and *Pseudomonadales sp.* (50%) and *Lactobacillales sp.* (22%), respectively.

Sediment and Solution Reactions in the 75 °C Treatment. In the higher temperature experiment, XRD on sediments revealed the main change from the start of the experiment was the dissolution of gypsum (SI Figure 5). Although by the end of the experiment the relative abundance of minerals had changed, there was no evidence that new minerals were present.

The production of sulfide was observed in both the higher temperature "live" treatments, starting around day 8 of each experiment. The sulfide production persisted in the poised trial until the end of the experiment, while the sulfide in the unpoised trial returned to abiotic levels by the point of sampling on day nine.

The 75 °C Experiment: Electrode Deposition. The live high-temperature treatment with the poised electrode yielded the greatest abundance of metal sulfide deposition (as measured by XRF; Figure 2), including sphalerite, chalcopyrite, marcasite, and pyrite (Table 1). The "dead" treatment with the poised electrode had the second most abundant metal sulfide deposition though the total deposition was substantially less, ~25% of that observed on the live treatment, using iron as a proxy for total deposition (Figure 2). This was also readily observable via SEM, where the abundance of copper and iron containing sulfides was readily apparent, and XRD, which confirmed chalcopyrite, sphalerite marcasite, and pyrite on the electrode (Table 1). The open-circuit electrodes from the live

DOI: 10.1021/acsearthspacechem.7b00042
ACS Earth Space Chem. 2017, 1, 277–287

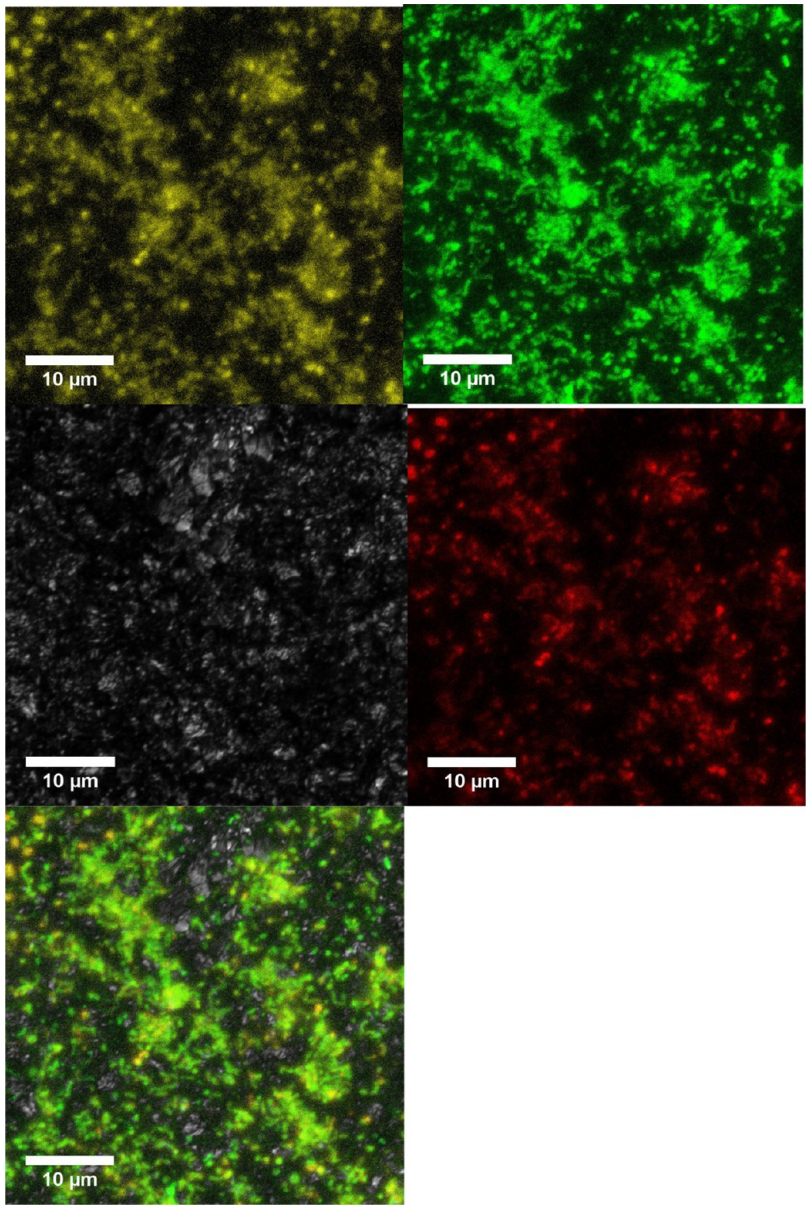

Figure 5. CLSM images from the live, poised, 75 °C trial. Left to right, top to bottom: lipids (fm464), DNA (syto9), reflection (405 nm), polysaccharides (wga555), and a composite.

and dead treatments had even less mineral deposition, with the open-circuit electrode from the dead treatment exhibiting mostly calcium carbonate deposition (SI Figure 6), and the open-circuit electrode from the live treatment exhibiting the least deposition of all trials. No diffraction patterns (other than graphite) were observed on the two open circuit electrodes.

Current production in the poised, live experiment began around day five (data not shown until day eight due to a computer logging malfunction) and persisted at milliamp levels until the end of the experiment. Current in the poised, dead treatment remained around 50 microamps for the entirety of the experiment, with the exception of brief spikes during sulfide additions (Figure 6). When converted to current per surface area, the maximum current produced in the live experiment is ~1100 mA/m^2 ; this is within the range previously reported for microbial fuel cells, which ranged from 44 to 6000 mA/m^2.[27]

Electrode Biofilm and Microbial Community Composition at 75 °C. The poised electrode from the live high-temperature treatment was coated with a substantial biofilm, several microns thick, and in certain locations extending off the surface of the electrode (Figure 4). Fluorescence microscopy of the biofilm demonstrated stain binding to lipids (fm464), DNA (syto9), and polysaccharides (wga555; Figure 5). Microbial morphologies observed to participate in the biofilm include spheres, rods and corkscrews. Although metal sulfides coat the surface of the electrode concomitant with the biofilm and are integrated throughout the biofilm, there is no obvious association or orientation of the cells toward the minerals as opposed to the graphite substrate. There also does not seem to be obvious pitting or tunneling into the minerals. The open circuit, live electrode exhibits several cells that are attached to the electrode surface individually; no biofilm was observed.

The library representing the electrode community in the 75 °C experiment was dominated by Deferribacterales (>97% of the reads returned) (Figure 1b). Deferribacterales was also a major fraction within the fluid (43%) and sediment (41% and

DOI: 10.1021/acsearthspacechem.7b00042
ACS Earth Space Chem. 2017, 1, 277−287

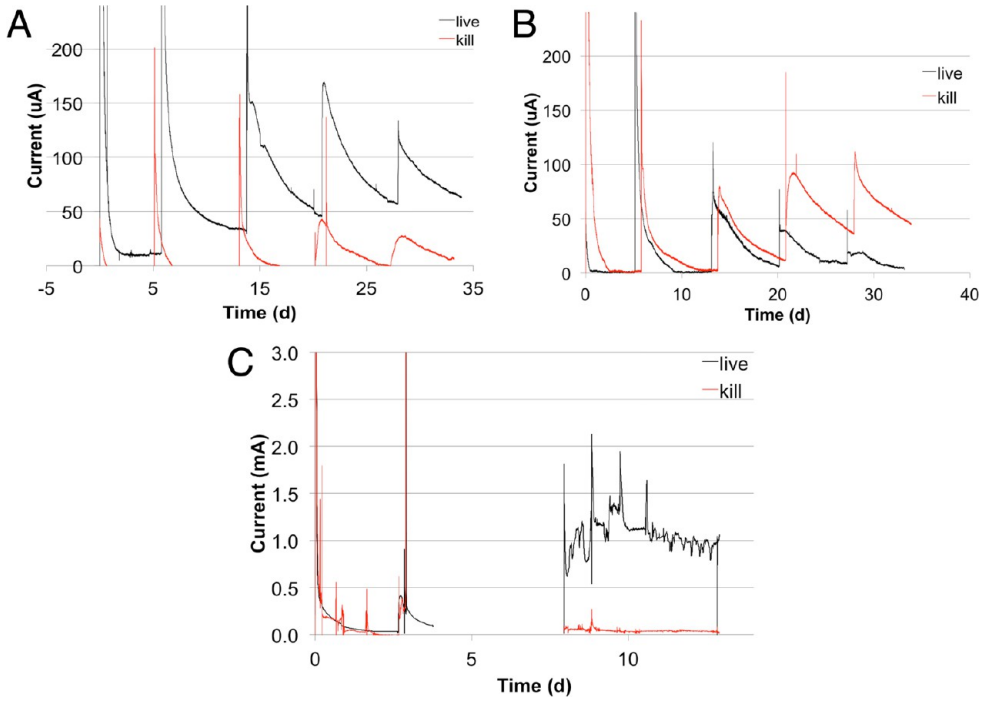

Figure 6. Current data for the live and kill experiments at (A) 195 mV and 30°C, (B) 218 mV and 30 °C, and (C) 195 mV and 75 °C.

44% for two extractions) of those reactors. The fluid of the open circuit, live experiment at 75 °C was also enriched in Deferribacterales (94%), thought to be allied to *Deferribacter desulfuricans* (via QIIME and RTL analyses[21]).

DISCUSSION

Biological and Chemical Controls on Mineral−Mineral Adhesion. Among all the experiments, the live treatments containing poised electrodes exhibited far more metal sulfide deposition than dead or open circuit systems. On the basis of morphology, size, and similarity to the minerals existing in the initial sediment inoculum, the metal sulfides attached to the electrode surface are most consistent with sorption of sulfide minerals that were added to the reactor, and came into contact with the electrode as the system stirred and not the result of de novo mineral growth in the reactors. That deposition was not observed in the live, open circuit treatments or the dead, poised treatments and the repetition of this observation twice at 30 °C and once at 75 °C (where different microbial communities were enriched) suggests that the result is based on the commonality of microbial activity and positive potential of these reactors. In addition, the preferential deposition of metal sulfides on the poised electrode surfaces, rather than the broad deposition of sulfates and other minerals that were most abundant in the reactor, indicates that metal sulfides are specifically influenced by the combined influences of the positive potential and the presence of active microorganisms associated with the electrode.

It has been demonstrated experimentally that the negatively charged bacterial surface can attract and concentrate positively charged metal ions.[28] Heavy metal ions tend to sorb to cell surfaces, mineral surfaces, and glycoconjugate matrices, rather than iron oxide minerals when all are in solution.[29] However, metal sulfides, including pyrite, sphalerite and chalcopyrite exhibit a pH_{IEP} below 3; in contrast to metal ions, they will be negatively charged in solution near circumneutral pH.[30] This would seem to suggest the possibility of metal sulfide sorption to the electrode in the absence of bacterial activity. However, this is not apparent in these data.

Although the surface charge of pure, synthesized or natural metal sulfides should be negative at the pH values of the experiment, it has been demonstrated that solution characteristics, including organics and bacterial activity, can vary the pH_{IEP} of minerals. For greigite and pyrrhotite, it has been demonstrated[31] that the addition of sulfide, humic acids, or a combination of the two changed the surface charge of these minerals from negative to positive at circumneutral pH. Similarly, the results in ref 32 showed an increase in the isoelectric point of chalcopyrite and pyrite after incubation with *Thiobacillus ferrooxidans*, potentially due to oxidation of the mineral surfaces, or bacterially generated organic material. *Deferribacter desulfuricans*, which is closely allied to the dominant species in the 75 °C experiment is a sulfur, nitrate, and arsenate reducing thermophile isolated from the Izu-Bonin Arc.[33] SRB have been demonstrated to produce EPS with a variety of functional groups which have been suggested to mediate the morphology and mineralogy of carbonate minerals and have both calcium and iron binding capacity.[34] It is not clear what the biological effect on carbonate minerals was in this study, although it seems that for the 30 °C system the live trials (both poised and open circuit) had more precipitation of calcium carbonate on the electrode (SI Figure 6), whereas the poised, kill systems had more in the sediments (SI Figure 5). In the 75 °C trial, XRF indicates the presence of some calcium on the electrode, however no calcium containing minerals were identified via XRD.

It is interesting that the increase in mineral−electrode attachment occurred in the presence of a lush biofilm as well as more modest microbial colonization, as it might be proposed that a biofilm should be responsible for more surface area and material to entrap minerals,[35] and the biofilm represents an extensively chemically modified microenvironment compared

DOI: 10.1021/acsearthspacechem.7b00042
ACS Earth Space Chem. 2017, 1, 277−287

to the rest of the reactor.[36] One possible explanation could be if a specific microbial metabolite is responsible for the adhesion—polysaccharides make up only ~1−2% of the biofilm matrix[37] and so could potentially contribute to adhesion even if present in small volumes. The fluorescence microscopy results (Figure 5) demonstrate that both lipids and polysaccharides are present on the electrode surface in the 75 °C trial. In addition, it is possible that a biofilm, or a greater number of cells, was present on the two 30 °C electrodes and was simply not observed on the section we used for microscopy. The community phylogenetic analyses from the electrode poised at 218 mV potentially supports this supposition, as the results from RTL found that the Campylobacterales enriched at 218 mV may be allied to *Sulfurospirillum* spp., that can reduce elemental sulfur and potentially other compounds such as thiosulfate, nitrate, selenate, or arsenate and does not grow at oxygen concentrations above 4%, fitting the experimental conditions of the working reactor.[38−40] Community phylogenetic analyses from the 30 °C electrode poised at 195 mV also support this assumption, as the order *Chromatiales* is comprised of purple sulfur bacteria. The enrichment of *Chromatiales* (sulfide oxidizing bacteria) and potentially *Sulfurospirillum sp.* (sulfur reducing bacteria) in the poised experiments at 30 °C, coupled with the presence of elemental sulfur on the electrodes (Table 1) and possible polysulfide formation (Results) is consistent with the idea that active sulfur cycling is occurring in the 30 °C reactors; this does not appear to be coupled to EET based upon the current results (Figure 6). The potentials of the poised reactors support spontaneous sulfide oxidation,[41] and our addition of lactate as a carbon source may have inadvertently biased the enrichment toward sulfur reducers (medium DSMZ was developed for *Desulfobacter sp.*). The enrichment of Deferribacteriales in the 75 °C experiment is also in keeping with sulfur reduction as a metabolism. In the 75 °C poised experiment, the high current production in the live experiment relative to the kill control (Figure 6) suggests microbial use of the electrode as an electron sink. The Deferribacteriales are also enriched in the high temperature open circuit experiment and in this case may be using elemental sulfur, rather than the electrode, as an electron acceptor. Although we did not observe elemental sulfur on the high-temperature electrodes (Table 1), as stated above, it could have formed via sulfide oxidation at our working potentials.

Alhough we observed differences in cell density on the electrodes between the poised and open circuit experiments, it is not clear that potential influenced beta diversity substantially as all high-temperature experiments are closely clustered via beta diversity analysis; SI Figure 4. The phenomenon of metal sulfide adhesion was only observed in the poised, live experiment (Figure 2) despite the enrichment of comparable microbial OTUs in both poised and open circuit experiments at 75°C, suggesting a role for electrostatic potential in addition to microbial enrichment. Finally, the difference in current produced (Figure 6) and microbial growth as visible via SEM and CLSM (Figures 3, 4, and 5) between the two temperature regimes (30 and 75 °C) is in keeping with previous finding of increased microbial activity at higher temperatures, specifically in terms of hydrothermal metabolisms.[7,8] The presence of some archaeal species in the 75 °C reactor is also consistent with increased archaeal abundance toward the higher temperature chimney center.[5]

Implications for Natural Systems. The electrochemical potential and current flow at hydrothermal vents will vary based upon the system chemistry, temperature, and the spatial location on the chimney where it is measured, as well as the mineral matrix through which electrons have been conducted at the point of measurement. In a previous study, a difference of 517 mV was measured between an artificially created 309 °C hydrothermal fluid and surrounding 4 °C seawater.[42]

If hydrophobicity and zeta potential are taken to be the most important parameters influencing bacterial cell-mineral adhesion[43] and the bacteria are capable of modifying these parameters on both their own surfaces and the mineral surfaces,[32] these could be viable explanations for the metal sulfide-electrode deposition observed in these experiments. In addition to changing the isoelectric point of the mineral, it was observed[32] that *T. ferrooxidans* grown in the presence of minerals were more hydrophobic than those grown in the presence of iron ions and suggested that a new proteinaceous surface component was responsible for the change. However, the extension from BES reactor to hydrothermal chimney is not straightforward, even though the general fluid chemistry of the hydrothermal vent chimney environment was approximated in this experiment. In the vent zone, pH, Eh, and often ionic strength will change as a result of variations in fluid flow, which is in contrast to conditions in the BES where changes in these parameters was gradual over the course of the experiment (SI Figure 7). Fluid flow characteristics also influence bacterial attachment and biofilm formation, for example, changing the thickness of the biofilm.[44] In addition, in the hydrothermal chimney environment the utility of electrostatic sorption interactions may be limited by the changes in pH. If carboxyl and phosphoryl functional groups are considered the most important for microbial−mineral adhesion, a pH change between 4.5 and 5.5, conceivable for the chimney, would cover the pK_a of both groups.[45] If the mineral sorption is only electrostatic, then a pH change should result in desorption unless accompanied by physical entrainment; if it does not, this is in keeping with the irreversibility of bacterial attachment.[44,46] Physical entrainment within the biofilm was sometimes visible for small sulfide minerals within the biofilm formed at 75 °C (Figure 4); in the low temperature experiments (30 °C), no biofilm was identified so no physical entrainment, nor spatial association between cells and minerals, was observed (Figure 3).

In considering the role of microbes in the development of vent chimneys, any influence of cell−mineral adhesion on the mineral attachment to other minerals (and therefore the chimney morphology) would occur later in chimney growth, as the initial structures are primarily composed of anhydrite (which forms at a minimum of 150°C[47]) and fluid temperatures are well above those known to support life (121°C[48]). As a result, microbial influence is limited to later stages of mineral deposition, subsequent to microbial colonization.

■ CONCLUSION

The present study demonstrates not just the adhesion of bacteria to minerals as previously described but also the adhesion of one mineral to another, conductive graphite to semiconductive metal sulfides, through the influence of bacteria in the presence of an applied electric potential. As electric potentials are common across natural environments, including hydrothermal vents, this result implies that parallel processes may be occurring in the natural environment. Despite the dominance of high temperature mineral forming reactions in these systems, this work demonstrates that microbes may have

DOI: 10.1021/acsearthspacechem.7b00042
ACS Earth Space Chem. 2017, 1, 277−287

a role in assembling natural mineral composites, such as hydrothermal vent chimneys, through mineral entrainment and adhesion, and extend the possibility that previously unconsidered biological processes influence otherwise abiotic mineral structures.

■ ASSOCIATED CONTENT

Supporting Information

The Supporting Information is available free of charge on the ACS Publications website at DOI: 10.1021/acsearthspacechem.7b00042.

Photograph of the experimental setup (SI Figure 1), SEM (SI Figure 2) of initial inoculum; full microbial community composition from 16S rRNA gene analysis (SI Figure 3); beta diversity analysis for all experiments (SI Figure 4); XRD results of sediments (SI Figure 5); XRF results of calcium (SI Figure 6); a schematic contrasting BES with natural hydrothermal chimneys (SI Figure 7) (PDF)

■ AUTHOR INFORMATION

Corresponding Authors

*E-mail: agartman@usgs.gov.
*E-mail: pgirguis@oeb.harvard.edu.

ORCID

A. Gartman: 0000-0001-9307-3062

Present Address

§(A.G.) U.S. Geological Survey, 2885 Mission Street, Santa Cruz, CA 95060, U.S.A.

Notes

The authors declare no competing financial interest.

■ ACKNOWLEDGMENTS

This work was performed in part at the Center for Nanoscale Systems (CNS), a member of the National Nanotechnology Coordinated Infrastructure Network (NNCI), which is supported by the National Science Foundation under NSF Award No. 1541959. CNS is part of Harvard University. Optical microscopy was performed at the Harvard Center for Biological Imaging (HCBI). XRD was performed at the Harvard Department of Chemistry and Chemical Biology X-ray Laboratory We would like to thank the staff of the CHNS and the HCBI and Shao-Liang Zheng at the X-ray Laboratory for training and support. We would also like to thank the HOV Alvin and Atlantis crew of AT26-23 for sample collection. Mahalo nui to Dr. Kiana Frank for providing the beta-diversity analysis. This work was supported by the National Science Foundation Grant 1344241.

■ REFERENCES

(1) Haymon, R. H. Growth history of hydrothermal black smoker chimneys. *Nature* **1983**, *301*, 695−698.
(2) Tivey, M. K.; Singh, S. Nondestructive imagining of fragile seafloor vent deposit samples. *Geology* **1997**, *25* (10), 931−934.
(3) Spagnoli, G.; Hannington, M.; Bairlein, K.; Hördt, A.; Jegen, M.; Petersen, S.; Laurila, T. Electrical properties of seafloor massive sulfides. *Geo-Mar. Lett.* **2016**, *36*, 235−245.
(4) Nakamura, R.; Takashima, T.; Kato, S.; Takai, K.; Yamamoto, M.; Hashimoto, K. Electrical Current Generation across a Black Smoker Chimney. *Angew. Chem.* **2010**, *122*, 7858−7860.
(5) Schrenk, M. O.; Kelley, D. S.; Delaney, J. R.; Baross, J. A. Incidence and Diversity of Microorganisms within the Walls of an Active Deep-Sea Sulfide Chimney. *Appl. Environ. Microbiol.* **2003**, *69* (6), 3580−3592.
(6) Toner, B. M.; Lesniewski, R. A.; Marlow, J. J.; Briscoe, L. J.; Santelli, C. M.; Bach, W.; Orcutt, B. N.; Edwards, K. J. Mineralogy Drives Bacterial Biogeography of Hydrothermally Inactive Seafloor Sulfide Deposits. *Geomicrobiol. J.* **2013**, *30* (4), 313−326.
(7) LaRowe, D. E.; Dale, A. W.; Aguilera, D. R.; L'Heureux, I.; Amend, J. P.; Regnier, P. Modeling microbial reaction rates in a submarine hydrothermal vent chimney wall. *Geochim. Cosmochim. Acta* **2014**, *124*, 72−97.
(8) Frank, K. L.; Rogers, D. R.; Olins, H. C.; Vidoudez, C.; Girguis, P.R. Characterizing the distribution and rates of microbial sulfate reduction at Middle Valley hydrothermal vents. *ISME J.* **2013**, *7*, 1391−1401.
(9) Olins, H. C.; Rogers, D. R.; Frank, K. L.; Vidoudez, C.; Girguis, P. R. Assessing the influence of physical, geochemical and biological factors on anaerobic microbial primary productivity within hydrothermal vent chimneys. *Geobiology.* **2013**, *11*, 279−293.
(10) Gralnick, J. A.; Newman, D. K. Extracellular respiration. *Mol. Microbiol.* **2007**, *65* (1), 1−11.
(11) Lovley, D. R. Electromicrobiology. *Annu. Rev. Microbiol.* **2012**, *66*, 391−409.
(12) Rowe, A. R.; Chellamuthu, P.; Lam, B.; Okamoto, A.; Nealson, K. H. Marine sediments microbes capable of electrode oxidation as a surrogate for lithotrophic insoluble substrate metabolism. *Front. Microbiol.* **2015**, *5*, 784.
(13) Sato, M.; Mooney, H. M. The electrochemical mechanism of sulfide self-potentials. *Geophysics* **1960**, *25* (1), 226−249.
(14) Reimers, C. E.; Girguis, P.; Stecher, H. A., III.; Tender, L. M.; Ryckelynck, N. Whaling, P. Microbial fuel cell energy from an ocean cold seep. *Geobiology* **2006**, *4*, 123−126.
(15) Nielsen, M. E.; Reimers, C. E.; White, H. K.; Sharma, S.; Girguis, P. R. Sustainable energy from deep ocean cold seeps. 2008. *Energy Environ. Sci.* **2008**, *1*, 584−593.
(16) Girguis, P. R.; Holden, J. F. On the potential for bioenergy and biofuels from hydrothermal vent microbes. *Oceanography* **2012**, *25* (1), 213−217.
(17) Hamilton, I. C.; Woods, R. An investigation of surface oxidation of pyrite and pyrrhotite by linear potential sweep voltammetry. *J. Electroanal. Chem. Interfacial Electrochem.* **1981**, *118*, 327−343.
(18) Widdel, F.; Bak, F. Gram-negative mesophilic sulfate-reducing bacteria. In *The Prokaryotes*; Balows, A., Trüper, H., Dworkin, M., Harder, W., Schleifer, K-H., Eds.; Springer: New York, 1992; pp 3352−3378.
(19) Santelli, C. S.; Orcutt, B. N.; Banning, E.; Bach, W.; Moyer, C. L.; Sogin, M. L.; Staudigel, H.; Edwards, K. J. Abundance and diversity of microbial life in ocean crust. *Nature* **2008**, *453*, 653−657.
(20) Caporaso, J. G.; Lauber, C. L.; Walters, W. A.; Berg-Lyons, D.; Huntley, J.; Fierer, N.; Owens, S. M.; Betley, J.; Fraser, L.; Bauer, M.; Gormley, N.; Gilbert, J. A.; Smith, G.; Knight, R. Ultra-high-throughput microbial community analysis on the Illumina HiSeq and MiSeq platforms. *ISME J.* **2012**, *6*, 1621−1624.
(21) Edgar, R. C. UPARSE: highly accurate OTU sequences from microbial amplicon reads. *Nat. Methods* **2013**, *10*, 996−998.
(22) Caporaso, J. G.; Bittinger, K.; Bushman, F. D.; DeSantis, T. Z.; Andersen, G. L.; Knight, R. PyNAST: a flexible tool for aligning sequences to a template alignment. *Bioinformatics* **2010**, *26*, 266−267.
(23) Edgar, R. C. Search and clustering orders of magnitude faster than BLAST. *Bioinformatics* **2010**, *26* (19), 2460−2461.
(24) DeSantis, T. Z.; Hugenholtz, P.; Larsen, N.; Rojas, M.; Brodie, E. L.; Keller, K.; Huber, T.; Dalevi, D.; Hu, P.; Andersen, G. L. Greengenes, a chimera-checked 16S rRNA gene database and workbench compatible with ARB. *Appl. Environ. Microbiol.* **2006**, *72* (7), 5069−5072.
(25) Schloss, P. D.; Westcott, S. L.; Ryabin, T.; Hall, J. R. A.; Hartmann, M.; Hollister, E. B.; Lesniewski, R. A.; Oakley, B. B.; Parks, D. H.; Robinson, C. J.; Sahl, J. W.; Stres, B.; Thallinger, G. G.; Van Horn, D. J.; Weber, C. F. Introducing mothur: open source, platform-independent, community-supported software for describing and

DOI: 10.1021/acsearthspacechem.7b00042
ACS Earth Space Chem. 2017, 1, 277−287

comparing microbial communities. *Appl. Environ. Microbiol.* **2009**, *69*, 3580−3592.
(26) Ondov, B. D.; Bergman, N. H.; Phillippy, A. M. 2011. Interactive metagenomic visualization in a Web browser. *BMC Bioinformatics* **2011**, *385* (12), 1471−2105.
(27) Nevin, K. P.; Richter, H.; Covalla, S. F.; Johnson, J. P.; Woodard, T. L.; Orloff, A. L.; Jia, H.; Zhang, M.; Lovley, D. R. Power output and columbic efficiencies from biofilms of *Geobacter sulfurreducens* comparable to mixed community microbial fuel cells. *Environ. Microbiol.* **2008**, *10* (10), 2505−2514.
(28) Beveridge, T. J. Role of cellular design in bacterial metal accumulation and mineralization. *Annu. Rev. Microbiol.* **1989**, *43*, 147−171.
(29) Hao, L.; Guo, Y.; Byrne, J. M.; Zeitvogel, F.; Schmid, G.; Ingino, P.; Li, J.; Neu, T. R.; Swanner, E. D.; Kappler, A.; Obst, M. Binding of heavy metal ions in aggregates of microbial cells, EPS and biogenic iron minerals measured in-situ using metal- and glycoconjugates-specific fluorophores. *Geochim. Cosmochim. Acta* **2016**, *180*, 66−96.
(30) Bebie, J.; Schoonen, M. A. A.; Fuhrmann, M.; Strongin, D. R. Surface charge development on transition metal sulfides: An electrokinetic study. *Geochim. Cosmochim. Acta* **1998**, *62* (4), 633−642.
(31) Dekkers, M. J.; Schoonen, M. A. A. An electrokinetic study of synthetic greigite and pyrrhotite. *Geochim. Cosmochim. Acta* **1994**, *58* (19), 4147−4153.
(32) Devasia, P.; Natarajan, K. A.; Sathyanarayana, D. N.; Ramandana, R. G. Surface Chemistry of *Thiobacillus ferrooxidans* Relevant to Adhesion on Mineral Surfaces. *Appl. Environ. Microbiol.* **1993**, *59* (12), 4051.
(33) Takai, K.; Kobayashi, H.; Nealson, K. H.; Horikoshi, K. *Deferribacter desulfuricans* sp. nov., a novel sulfur-, nitrate- and arsenate-reducing thermophile isolated from a deep-sea hydrothermal vent. *Int. J. Syst. Evol. Microbiol.* **2003**, *53*, 839−836.
(34) Braissant, O.; Decho, A. W.; Dupraz, C.; Glunk, C.; Przekop, K. M.; Visscher, P. T. Exopolymeric substances of sulfate-reducing bacteria: Interactions with calcium at alkaline pH and implication for formation of carbonate minerals. *Geobiology* **2007**, *5*, 401−411.
(35) Sutherland, I. W. Biofilm exopolysaccharides: a strong and sticky framework. *Microbiology* **2001**, *147*, 3−9.
(36) Decho, A. W. Overview of biopolymer-induced mineralization: What goes on in biofilms? *Ecol. Eng.* **2010**, *36*, 137−144.
(37) Sutherland, I. W. The biofilm matrix- an immobilized but dynamic microbial environment. *Trends Microbiol.* **2001**, *9* (5), 222−227.
(38) Stolz, J. F.; Ellis, D. J.; Switzer Blum, J.; Ahmann, D.; Lovley, D. R.; Oremland, R. S. Sulfurospirillum barnesii sp. mov. And Sulfurospirillum arsenophilum sp. nov., new members of the Sulfurospirilllum clade of the ε Proteobacteria. *Int. J. Syst. Bacteriol.* **1999**, *49*, 1177−1180.
(39) Stolz, J. F.; et al. Sulfurospirillum. *Bergey's Manual of Systematics of Archaea and Bacteria* **2015**, 1−7.
(40) Rabus, R.; Hansen, T. A.; Widdel, F. Dissimilatory Sulfate- and Sulfur-Reducing Prokaryotes. In *Prokaryotes*; Falkow, S., Rosenberg, E., Schleifer, K. H., Stackebrandt, E., Eds.; Springer: New York, 2006; pp 659−768.
(41) Rabaey, K.; Van de Sompel, K.; Maignien, L.; Boon, N.; Aelterman, P.; Clauwaert, P.; De Schamphelaire, L.; Pham, H. T.; Vermeulen, J.; Verhaege, M.; Lens, P.; Verstraete, W. Microbial Fuel Cells for Sulfide Removal. *Environ. Sci. Technol.* **2006**, *40* (17), 5218−5224.
(42) Yamamoto, M.; Nakamura, R.; Oguri, K.; Kawagucci, S.; Suzuki, K.; Hashimoto, K.; Takai, K. Generation of Electricity and Illumination by an Environmental Fuel Cell in Deep-Sea Hydrothermal Vents. *Angew. Chem., Int. Ed.* **2013**, *52*, 10758−10761.
(43) van Loosdrecht, M. C. M.; Lyklema, J.; Norde, W.; Schraa, G.; Zehnder, A. J. B. Electrophoretic Mobility and Hydrophobicity as a Measure To Predict the Initial Steps of Bacterial Adhesion. *Appl. Environ. Microbiol.* **1987**, *53* (8), 1898−1901.
(44) Katsikogianni, M.; Missirlis, Y. F. Concise review of mechanisms of bacterial adhesion to biomaterials and of techniques used in estimating bacteria-material interactions. *Eur. Cell. Mater.* **2004**, *8*, 37−57.
(45) Stumm, W., Morgan, J. J. *Aquatic Chemistry: Chemical Equilibria and Rates in Natural Waters*, 3rd, ed.; Wiley: New York, 1996.
(46) Rijnaarts, H. H. M.; Norde, W.; Bouwer, E. J.; Lyklema, J.; Zehnder, A. J. B. Reversibility and mechanism of bacterial adhesion. *Colloids Surf., B* **1995**, *4*, 5−22.
(47) Bischoff, J. L.; Seyfried, W. E. Hydrothermal Chemistry of Seawater from 25° to 350°C. *Am. J. Sci.* **1978**, *278*, 838−860.
(48) Kashefi, K.; Lovley, D. R. Extending the Upper Temperature Limit for Life. *Science* **2003**, *301* (5635), 934.

DOI: 10.1021/acsearthspacechem.7b00042
ACS Earth Space Chem. 2017, 1, 277−287